ISSN 1392-1207. MECHANIKA. Vol. 30, No. 1, 2024: 23–28

Multiscale Elastohydrodynamic Wedge-Platform Thrust Bearing with Ultra Low Clearance

Chao WANG*, **, Yongbin ZHANG***
**College of Mechanical Engineering, Changzhou University, Changzhou, Jiangsu Province, China*
***Jiangsu Power Equipment Co., Ltd., Changzhou, Jiangsu Province, China*
****College of Mechanical Engineering, Changzhou University, Changzhou, Jiangsu Province, China,*
E-mails: yongbinzhang@cczu.edu.cn, engmech1@sina.com (Corresponding Author)
https://doi.org/10.5755/j02.mech.34137

1. Introduction

In the analysis of hydrodynamic thrust bearings, the surfaces were often assumed as rigid because of the magnitude of the surface elastic deformation far lower than the bearing clearance owing to low hydrodynamic film pressures [1-4]. There have been also the researches on these bearings by considering the surface elastic deformation in the condition of relatively heavy loads and low sliding speeds [5, 6]. In the big-size hydrodynamic thrust bearings such as in hydrogenerators and turbo machines, the surface clearance can be ultra low or even vanishing [7, 8]. In the micro thrust bearings, the surface separations are intrinsically ultra low [9, 10]. It was found that when the surface separation is smaller than one hundred times of the thickness of the physically adsorbed layer on the bearing surface, the effect of the physically adsorbed layer in the bearing should be considered [11]. In a hydrodynamic thrust bearing, when the surface separation is ultra low, there will be the pure adsorbed layer area in the outlet zone, while in the remaining areas the sandwich flows occur consisting of both the adsorbed layer flow and the intermediate continuum fluid flow. By using the multiscale analysis, Wang and Zhang [12] studied the performance of the hydrodynamic wedge-platform thrust bearing working in this condition by assuming rigid surfaces. They showed that when the surface clearance in the outlet zone of this bearing is below 5nm, the hydrodynamic pressures can be increased by 2 orders by the effect of the adsorbed layer for the strong fluid-bearing surface interaction, compared to the classical calculations; The dimensional pressures in this bearing can be more than 100 MPa, so large as to cause the surface elastic deformation significantly greater than the surface clearance.

In the hydrodynamic thrust bearing with the ultra low clearance on the 1nm scale, it is conjectured that the resulting surface elastic deformation should often be comparable to or even greater than the surface separation, and the effect of the surface elastic deformation should often be pronounced. This now becomes a new research task. The present paper aims to study the effect of the surface elastic deformation in the hydrodynamic wedge-platform thrust bearing with ultra low clearance by using the multiscale approach. Interesting results have been obtained concerning the significant effects of the surface elastic deformation on both the film pressure distribution and the surface separation profile in this bearing, which strongly depends on the fluid-bearing surface interaction.

2. Studied bearing with surface elastic deformation

By considering both the surfaces as rigid, Wang and Zhang [12] studied the hydrodynamic wedge-platform thrust bearing with ultra low clearance where there are only the physically adsorbed layers (with the continuum fluid film vanishing) in the outlet zone, close to the outlet zone also only exist the physically adsorbed layers, and in the remaining area of the inlet zone occurs the sandwich film consisting of both the adsorbed layers and the intermediate continuum fluid. When both the surfaces are considered as elastic, this kind of lubrication mode may also exist except the reduced area of the pure adsorbed layer owing to the surface elastic deformation, as shown by Fig. 1, a. However, owing to the surface elastic deformation, the surface separations may be increased so that the sandwich film will occur in the whole hydrodynamic area of the bearing, as shown by Fig. 1, b; This is another lubrication mode in the studied bearing. The present study addresses both of these two lubrication modes.

In Figs. 1, a and b, h_{tot} is the surface separation, $h_{tot,o}$ is the surface separation on the exit of the bearing, h is

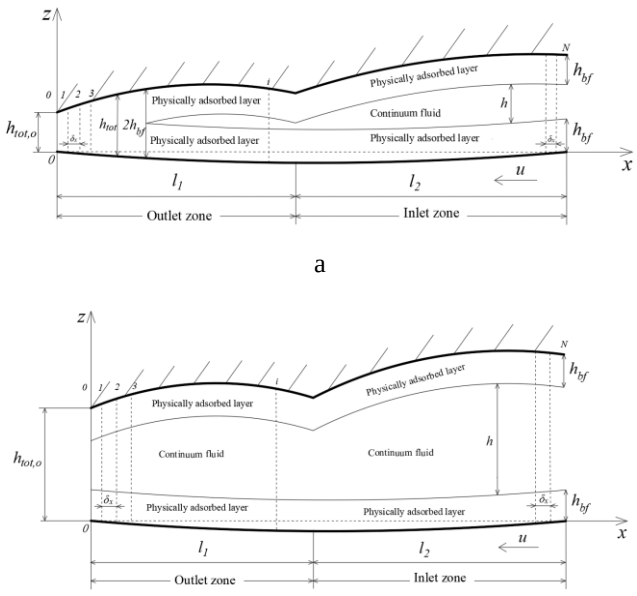

a

b

Fig. 1 The two lubrication modes in the hydrodynamic wedge-platform thrust bearing with ultra low clearance and surface elastic deformation: a - $h_{tot,o} < 2\ h_{bf}$, b - $h_{tot,o} > 2\ h_{bf}$

the continuum fluid film thickness, h_{bf} is the thickness of the adsorbed layer, l_1 and l_2 are respectively the widths of the outlet and inlet zones, and the coordinates are also shown.

3. Analysis

As done by Wang and Zhang [12], the present study uses the non-continuum nanoscale flow equation to describe the pure adsorbed layer flow and the multiscale flow equations to describe the flow of the sandwich film. By this way, the solution is sufficiently fast to satisfy the engineering sizes of the bearing.

The present analysis is based on the following assumptions:

a. two bearing surfaces are identical;
b. the side leakage is neglected;
c. the bearing surfaces are perfectly smooth;
d. no interfacial slippage occurs on any interface;
e. the condition is isothermal and steady-state.

3.1. Governing equations

Some mathematical equations are fundamental and may be repeated in this section. When the intermediate continuum fluid film is present between two adsorbed layers as shown by the sandwich film, the governing equation is [12]:

$$\frac{dp}{dx}=\frac{ah+d}{ch^3+b}, \tag{1}$$

where: $a=u\rho/2$, $d=q_m+u\rho_{bf,1}^{eff}h_{bf}$,

$$b=\frac{\rho_{bf,1}^{eff}h_{bf}^3}{\eta_{bf,1}^{eff}}\left[\frac{F_1}{6}-\left(1+\frac{1}{2\lambda_{bf}}-\frac{q_0-q_0^n}{q_0^{n-1}-q_0^n}\frac{\Delta_{n-2}}{h_{bf}}\right)\frac{\varepsilon}{1+\frac{\Delta x}{D}}\right], \tag{2}$$

$$c=\rho\left\{\frac{1}{\eta_{bf,1}^{eff}}\left[\frac{F_2\lambda_{bf}^2}{6}-\frac{\lambda_{bf}}{1+\frac{\Delta x}{D}}\left(\frac{1}{2}+\lambda_{bf}-\lambda_{bf}\frac{q_0-q_0^n}{q_0^{n-1}-q_0^n}\frac{\Delta_{n-2}/D}{h_{bf}/D}\right)\right]-\frac{1}{12\eta}\right\}, \tag{3}$$

here: $\lambda_{bf}=h_{bf}/h$, p is the hydrodynamic pressure, x is the coordinate in the flow direction, u is the sliding speed and positive, ρ and η are respectively the bulk density and the bulk viscosity of the fluid, $\rho_{bf,1}^{eff}$ and $\eta_{bf,1}^{eff}$ are respectively the average density and the effective viscosity of the physically adsorbed layer, D and Δx are respectively the fluid molecule diameter and the separation between the neighboring fluid molecules in the x coordinate direction in the adsorbed layer, $q_0=\Delta_{j+1}/\Delta_j$ (Δ_j is the separation between the $(j+1)^{\text{th}}$ and j^{th} fluid molecules across the adsorbed layer thickness) and q_0 is averagely constant, n is the equivalent number of the fluid molecules across the adsorbed layer thickness, Δ_{n-2} is the separation between the neighboring fluid molecules across the adsorbed layer thickness just on the boundary between the adsorbed layer and the continuum fluid film, and the formulations for F_1, F_2 and ε were shown in [12].

When the intermediate continuum fluid film is absent because of too small surface separations and there is thus only the physically adsorbed layer across the whole surface separation, the governing equation is [12]:

$$\frac{dp}{dx}=\frac{A}{h_{tot}^2}+\frac{Bq_m}{h_{tot}^3}, \tag{4}$$

where: $A=6u\eta_{bf,2}^{eff}/S$, $B=12\eta_{bf,2}^{eff}/\left(S\rho_{bf,2}^{eff}\right)$. $\rho_{bf,2}^{eff}$ and $\eta_{bf,2}^{eff}$ are respectively the average density and the effective viscosity of the adsorbed layer across the whole surface separation, and S is the parameter accounting for the non-continuum effect of the adsorbed layer.

3.2. Numerical calculation

Owing to the surface elastic deformation, the current problem is highly non-linear, and the numerical approach is mandatory for finding the solution. In the present calculation, there are evenly distributed (N+1) discretized points in the whole lubricated area in the bearing, as shown in Figs. 1, a and b.

3.2.1. Numerical analysis for the bearing

By forward difference, the pressure on the J^{th} discretized point is:

$$\left.\frac{dp}{dx}\right|_J=\frac{p_J-p_{J-1}}{\delta_x}=\begin{cases}\dfrac{a_Jh_J+d_J}{c_Jh_J{}^3+b_J} & \text{, for } h_J>0\\ \dfrac{A_J}{h_{tot,J}^2}+\dfrac{B_Jq_m}{h_{tot,J}^3}\text{, for } h_{tot,J}\le 2h_{bf}\end{cases} \tag{5}$$

for J = 1, 2…, N,
where: a_J, b_J, c_J, d_J, A_J and B_J are the values of the corresponding parameters on the J^{th} discretized point, p_J and p_{J-1} are respectively the pressures on the J^{th} and $(J-1)^{th}$ discretized points, and $\delta_x=(l_1+l_2)/N$.

Considering the surface elastic deformation, the surface separation on the J^{th} discretized point is expressed as:

$$h_{tot,J}=h_{oo}+f\left(x_J\right)-\frac{2}{\pi E_v}\int_0^{l_1+l_2}p(s)ln\left(x_J-s\right)^2ds, \tag{6}$$

where: h_{oo} is constant, E_v is the compound Young's modulus of elasticity of two bearing surfaces, and

$$f(x_J)=\begin{cases}0 & 0\le x_J\le l_1\\ (x_J-l_1)\tan\theta & l_1<x_J\le l_1+l_2\end{cases}, \quad (7)$$

here θ is the wedge angle of the bearing.

The thickness of the intermediate continuum fluid film on the J^{th} discretized point is:

$$h_J=h_{oo}+f(x_J)-\frac{2}{\pi E_v}\int_0^{l_1+l_2}p(s)ln(x_J-s)^2\,ds-2h_{bf}. \quad (8)$$

Based on the boundary condition $p_0 = 0$, the pressure on each discretized point was calculated step by step by using the following equation:

$$p_J=p_0+\sum_{k=1}^{J}(p_k-p_{k-1}), \quad (9)$$

for $J = 1, 2,\ldots, N$; where $(p_k - p_{k-1})$ is calculated from Eq. (5).

The load per unit contact length carried by the bearing is:

$$w=\delta_x\sum_{J=1}^{N-1}p_J\ . \quad (10)$$

4. Numerical calculation

4.1. Numerical integration

In Eqs. (6) and (8), there is the following integration:

$$\Theta_J=-\frac{2}{\pi E_v}\int_0^{l_1+l_2}p(s)ln(x_J-s)^2\,ds. \quad (11)$$

Because the pressure distribution $p(s)$ can not be formulated by the explicit function, this integration can only be numerically calculated by interpolating $p(s)$. Eq. (11) is thus approximately formulated as:

$$\Theta_J\approx\sum_{K=1}^{N-1}C_{JK}\,p_K, \quad (12)$$

where

$$C_{JK}=-\frac{2}{\pi E_v}\int_{\frac{x_{K-1}+x_K}{2}}^{\frac{x_{K+1}+x_K}{2}}ln(x_J-s)^2ds, \quad (13)$$

here, x_{K-1}, x_K and x_{K+1} are respectively the x coordinates of the $(K\text{-}1)^{th}$, K^{th} and $(K\text{+}1)^{th}$ discretized points. It is then found that:

$$\begin{aligned}C_{JK}=&-\frac{2}{\pi E_v}ln\left(\frac{x_{K+1}+x_K}{2}-x_J\right)^2\left(\frac{x_{K+1}+x_K}{2}-x_J\right)+\\&+\frac{2}{\pi E_v}ln\left(\frac{x_{K-1}+x_K}{2}-x_J\right)^2\left(\frac{x_{K-1}+x_K}{2}-x_J\right)+\\&+\frac{2}{\pi E_v}(x_{K+1}-x_{K-1}).\end{aligned} \quad (14)$$

4.2. Numerical solution procedure

Fig. 2 shows the numerical solution procedure used in the computer calculation. k_n is the order number of the iteration calculation; $p^{(0)}$, $h_{tot}^{(0)}$ and $w^{(0)}$ are respectively the hydrodynamic pressure, surface separation and bearing load calculated for rigid surfaces; $h_{tot,o,r}$ is the surface separation on the exit of the bearing calculated for rigid surfaces , $\Theta^{(k_n)}$ is the value of Θ in the k_n^{th} iteration; $p^{(k_n)}$ is the hydrodynamic pressure in the k_n^{th} iteration; $h_{tot}^{(k_n)}$ is the value of h_{tot} in the k_n^{th} iteration; ϑ is the relaxation factor; $w_{max}^{(1)}$ and $w_m^{(1)}$ are respectively the calculated bearing loads for elastic surfaces when $h_{oo} = h_{oo,max}$ and $h_{oo} = h_{oo,m}$. $Q_m^{(k_n+1)}$ is the dimensionless mass flow rate per unit contact length through the bearing obtained in the

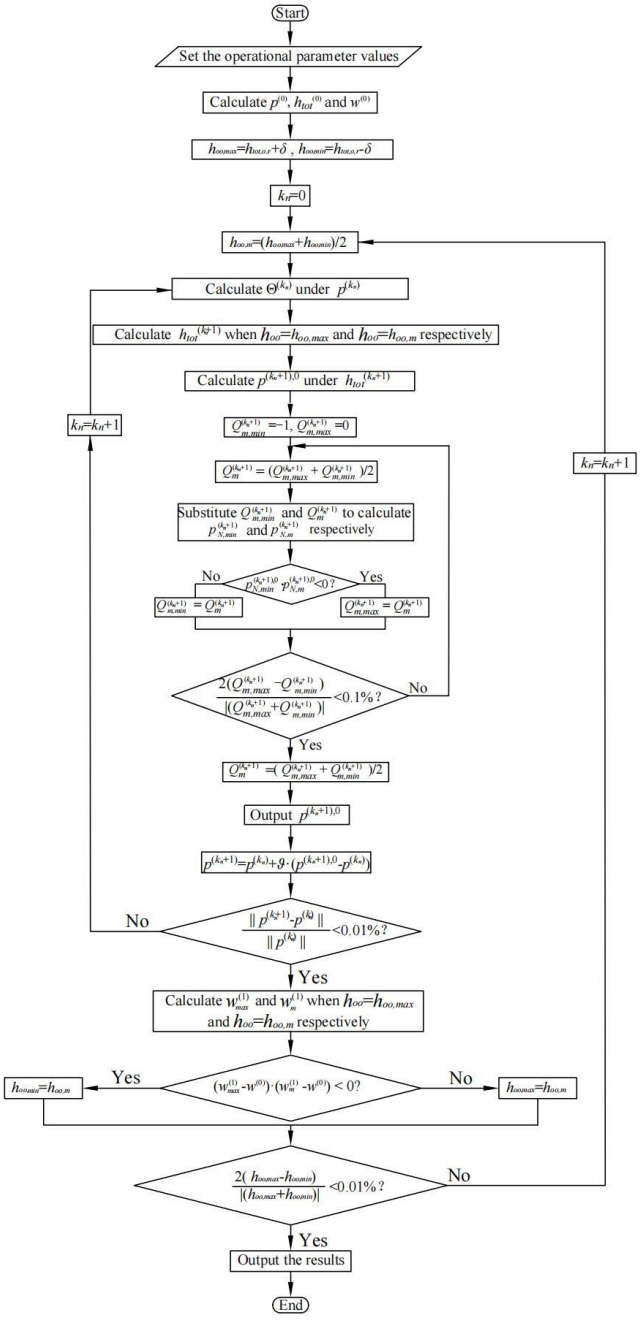

Fig. 2 The numerical solution procedure

$(k_n+1)^{th}$ iteration and it is satisfied that $Q_{m,min}^{(k_n+1)} \le Q_m^{(k_n+1)} \le Q_{m,max}^{(k_n+1)}$. Here, it is defined that $Q_m = q_m / u\rho_a h_{tot,o}$. Then, the pressures on all the discretized points can be calculated from the equations shown above, by starting the calculation from the exit of the bearing. $p_{N,min}^{(k_n+1),0}$ and $p_{N,m}^{(k_n+1),0}$ are respectively the hydrodynamic pressures on the entrance of the bearing when $Q_m^{(k_n+1)} = Q_{m,min}^{(k_n+1)}$ and $Q_m^{(k_n+1)} = (Q_{m,min}^{(k_n+1)} + Q_{m,max}^{(k_n+1)})/2$; The value of Q_m will be obtained when the following convergence criterion is satisfied: $2\left|(Q_{m,max}^{(k_n+1)} - Q_{m,min}^{(k_n+1)})/(Q_{m,max}^{(k_n+1)} + Q_{m,min}^{(k_n+1)})\right| < 0.1\%$.

4.3. Parameter formulation

According to the Roelands fluid viscosity-pressure relation [13], the bulk viscosity of the fluid film on the J^{th} discretized point is expressed as:

$$\eta_J = \eta_a \exp\left\{\left(\ln\eta_a + 9.67\right)\left[\left(1+5.1E-9\,p_{J-1}\right)^z - 1\right]\right\}, \quad (15)$$

where $z = \alpha / [5.1E\text{-}9(\ln\eta_a + 9.67)]$, η_a is the fluid bulk viscosity at ambient pressure, and α is constant.

At relatively low pressures, the dependence of the fluid bulk density on fluid pressure is nearly linear, and the bulk density of the fluid film on the J^{th} discretized point is expressed as:

$$\rho_J = \rho_a\left(1+\beta\cdot p_{J-1}\right), \quad (16)$$

where ρ_a the fluid bulk density at ambient pressure and β is constant.

Define $C_{y1}\left(H_{bf,1}\right) = \eta_{bf,1}^{eff} / \eta$ and $C_{q1}\left(H_{bf,1}\right) = \rho_{bf,1}^{eff} / \rho$, where $H_{bf,1} = h_{bf} / h_{cr,bf,1}$, and $h_{cr,bf,1}$ is the critical thickness for characterizing the rheological properties of the adsorbed layer in the sandwich film area. Define $C_{y2}(H_{bf,2}) = \eta_{bf,2}^{eff} / \eta$ and $C_{q2}(H_{bf,2}) = \rho_{bf,2}^{eff} / \rho$, where $H_{bf,2} = h_{tot} / h_{cr,bf,2}$, $h_{cr,bf,2}$ is the critical thickness for characterizing the rheological properties of the adsorbed layer which exists across the whole surface separation, and $h_{cr,bf,2} = 2h_{cr,bf,1}$. The equation formulations for $C_{q1}(H_{bf,1})$, $C_{q2}(H_{bf,2})$, $C_{y1}(H_{bf,1})$, $C_{y2}(H_{bf,2})$ and S have been shown in [12] and here are not repeated.

The weak, medium and strong fluid-bearing surface interactions were respectively considered. The operational parameter values for these interactions are the same with those shown in [12].

The other input operational parameter values are: D = 0.5 nm, N = 1000, $\Delta_{n-2} / D = \Delta x / D$ = 0.15, $l_1 = l_2$ = 100 μm, θ = 1E-4 rad, α = 1.6E-8 m^2/N, η_a = 0.03 Pa·s, β = 4E-10 Pa^{-1}, E_v = 2.09E+11 Pa, ϑ = 0.2.

5. Results

5.1. Effect of the surface elastic deformation on hydrodynamic pressure distribution

Figs. 3, a-c compare the hydrodynamic pressure distributions in the bearing calculated from the present multiscale approach respectively for elastic and rigid surfaces when the fluid-bearing surface interactions are weak, medium and strong. It is shown that the surface elastic deformation greatly changes the film pressure profile in the bearing although the film pressures may be no more than 2.4 MPa. This is especially significant for a strong fluid-bearing surface interaction. It indicates that the magnitude of the surface elastic deformation resulting from the low pressures is indeed comparable to the surface separation. The effect of the surface elastic deformation pronouncedly reduces the maximum film pressure, remarkably increases the film pressures in the outlet zone, but reduces the film pressures in the inlet zone. It appears to flatten the film pressure profile in the bearing.

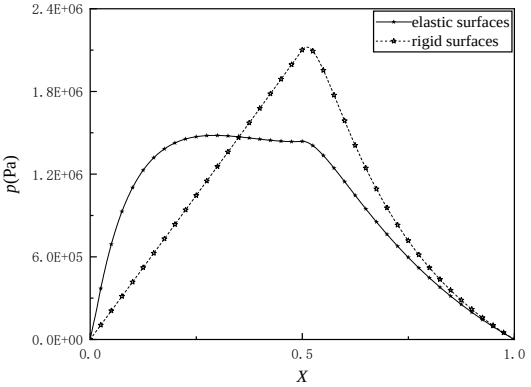

a

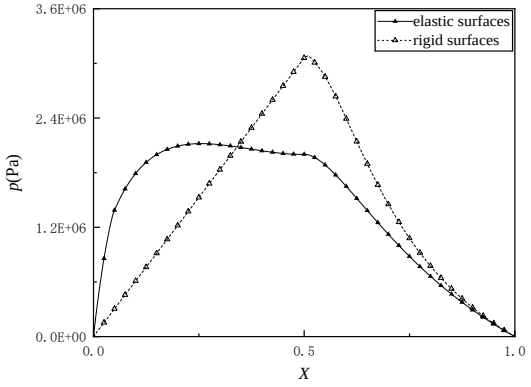

b

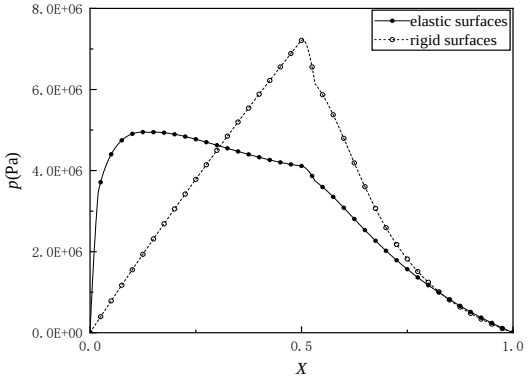

c

Fig. 3 Comparison of the film pressure distributions in the bearing calculated respectively for elastic and rigid surfaces for different fluid-bearing surface interactions when u = 1E-5 m/s: a - for the weak interaction, w = 192 N/m, b - for the medium interaction, w = 283 N/m, c - for the strong interaction, w = 622 N/m

5.2. Effect of the surface elastic deformation on the surface separation profile

Figs. 4, a-c compare the surface separation profiles in the bearing calculated respectively for elastic and rigid surfaces when the fluid-bearing surface interactions are weak, medium and strong. It is shown that the surface elastic deformation normally has a strong influence on the surface separation profile in the present bearing especially for a strong fluid-bearing surface interaction. We can notice the "end constriction" resulting from the surface elastic deformation. The effect of the surface elastic deformation is shown to increase the surface separations in the outlet zone including on the exit of the bearing (i.e. the minimum surface separation). The surface separation profiles in Figs. 4, a-c correspond to the film pressure profiles in Figs. 3, a-c. Figs. 4, a-c directly show the magnitude of the surface elastic deformation in the present bearing on the same scale with the surface clearance. It can be derived that if the film pressures are higher for higher sliding speeds or/and bigger bearing widths, the magnitude of the surface elastic deformation would be larger than the surface clearance, and this should bring much more significant effects of the surface elastic deformation in the bearing.

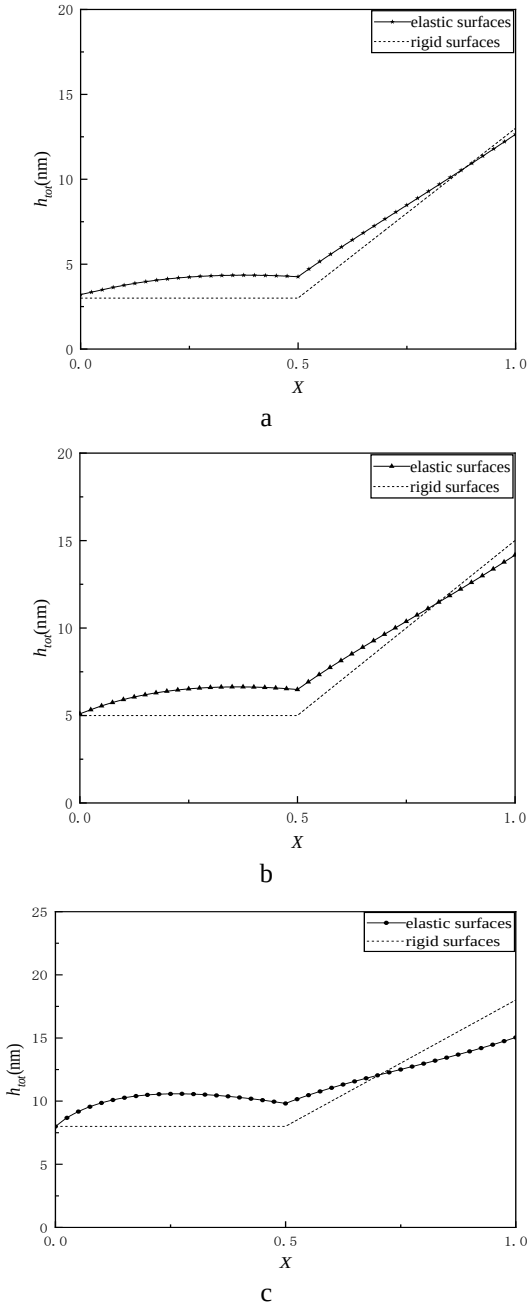

Fig. 4 Comparison of the surface separation profiles in the bearing calculated respectively for elastic and rigid surfaces for different fluid-bearing surface interactions when u = 1E-5 m/s: a - for the weak interaction, w = 192 N/m, b - for the medium interaction, w = 283 N/m, c - for the strong interaction, w = 622 N/m

6. Conclusions

The present paper investigates the effect of the surface elastic deformation in the hydrodynamic wedge-platform thrust bearing with the ultra low clearance on the 1nm scale by the multiscale analysis. Because of the surface elastic deformation, the lubrication status in this bearing may be apparently different from that for rigid bearing surfaces; The surface elastic deformation on the same scale with or significantly larger than the bearing clearance may result in the occurrence of the sandwich film in the whole lubricated area of the bearing which consists of both the adsorbed layers and the intermediate continuum fluid film. The surface elastic deformation expands the sandwich film area but reduces the pure adsorbed layer area with critically low surface separations.

The non-continuum nanoscale flow equation was used to simulate the flow of the adsorbed layer occurring across the whole surface separation. The multiscale flow equations were used to simulate both the adsorbed layer flows and the intermediate continuum fluid flow in the sandwich film area. The coupling of these equations gives an ultra fast solution for the engineering size of the bearing. Because of the highly non-linear problem resulting from the surface elastic deformation, the present solution can only be obtained by the numerical approach.

The caluations have been made for varying operational paramter values. The conclusions are drawn as follows:

a. The effect of the surface elastic deformaiton is normally very significant in the studied bearing;

b. The magnitude of the surface elastic deformation even resulting from low pressures is comparable to or on the same scale with the surface clearance in this bearing;

c. It is possible that the magnitude of the surface elastic deformation is much larger than the surface clearance in this bearing in the condition of higher sliding speeds or/and bigger bearing widths; In this case, the effect of the surface elastic deformation should be very strong;

d. The surface elastic deformation greatly changes both the film pressure profile and the surface separation profile in the bearing. It appears to flatten the film pressure profile by remarkably reducing the maximum film pressure. However, it increases both the film pressures and the surface separations in the outlet zone.

References

1. **Pinkus, O.; Sternlicht, B.** 1961. Theory of hydrodynamic lubrication, McGraw-Hill, New York.

2. **Wang, C. C.; Jyun-Ting, L.** 2022. Numerical study of hydrodynamic herringbone-grooved journal bearings combined with thrust bearings considering thermal effects, Journal of Mechanics 38: 13–21. https://doi.org/10.1093/jom/ufab036.
3. **Raymand, G. A.; Amalraj, I. J.** 2019. Inertia effects in rheodynamic lubrication of an externally pressurized converging thrust bearing using bingham fluids, Journal of Applied Fluid Mechanics 12: 587-594. https://doi.org/10.29252/jafm.12.02.28914.
4. **Agrawal, N.; Sharma; S. C.** 2023. Micro-grooved hybrid spherical thrust bearing with Non-Newtonian lubricant behaviour, International Journal of Mechanical Sciences 240: 107940. https://doi.org/10.1016/j.ijmecsci.2022.107940.
5. **Liang, X.; Han, M.; He, T.; Cui., L.; Yang, Z.; Ouyang, W.** 2023. A mixed lubrication deterministic model of an elastic support water-lubricated tilting pad thrust bearing, Lubricants 11(6): 262. https://doi.org/10.3390/lubricants11060262.
6. **Singh, U. P.** 2020. Mathematical analysis of effects of surface roughness on steady performance of hydrostatic thrust bearings lubricated with Rabinowitsch type fluids, Journal of Applied Fluid Mechanics 13(4): 1339-1347. https://doi.org/10.36884/JAFM.13.04.30682.
7. **Ettles, C. M.** 1980. Size effects in tilting pad thrust bearings, Wear 59(1): 231–245. https://doi.org/10.1016/0043-1648(80)90281-1.
8. **Kawaike, K.; Okano, K.; Furukawa, Y.** 1979. Performance of a large thrust bearing with minimized thermal distortion, ASLE Transactions 22(2): 125–134. https://doi.org/10.1080/05698197908982908.
9. **Ho, C. M.; Tai, Y. C.** 1998. Micro-electro-mechanical-systems (MEMS) and fluid flows, Annual Review of Fluid Mechanics 30(1): 579-612. https://doi.org/10.1146/annurev.fluid.30.1.579.
10. **Judy, J. W.** 2001. Microelectromechanical systems (MEMS): fabrication, design and applications, Smart Materials and Structures 10(6): 1115. https://doi.org/10.1088/0964-1726/10/6/301.
11. **Gu, K. C.; Shao, S. J.; Zhang, Y. B.** 2023. Multiscale analysis of hydrodynamic journal bearing considering the effect of the physically adsorbed boundary layer, International Journal of Automotive Technology 24: 335-345. https://doi.org/10.1007/s12239-023-0028-3.
12. **Wang, C.; Zhang, Y. B.** 2022. Analysis for hydrodynamic wedge-platform thrust slider bearing with ultra low surface separation, International Journal of Rotating Machinery 2022: 1-17. https://doi.org/10.1155/2022/8101357.
13. **Roelands, C. J. A.** 1966 Correlation aspects of the viscosity-temperature-pressure relationship of lubricating oils, PhD thesis, Delft University of Technology, Netherlands, Groningen.

C. Wang, Y. Zhang

MULTISCALE ELASTOHYDRODYNAMIC WEDGE-PLATFORM THRUST BEARING WITH ULTRA LOW CLEARANCE

S u m m a r y

The effect of the surface elastic deformation is investigated by the multiscale approach in the hydrodynamic wedge-platform thrust bearing with the ultra low clearance on the 1nm scale, by incorporating both the non-continuum pure adsorbed layer flow and the multiscale “sandwich” film flow. The pure adsorbed layer flow in ultra small surface separations is described by the non-continuum nanoscale flow equation; The “sandwich” film flow is described by the multiscale flow equations respectively for the adsorbed layer flow and the intermediate continuum fluid flow. The numerical calculation results show that in the studied bearing, the effect of the surface elastic deformation is normally significant, it pronouncedly reduces the maximum film pressure, greatly changes both the film pressure profile and the surface separation profile, and considerably increases the minimum surface separation, which occurs on the exit of the bearing. The effect of the surface elastic deformation is shown to be obviously dependent on the fluid-bearing surface interaction.

Keywords: adsorbed layer, elastic deformation, hydrodynamics, multiscale, pressure, thrust bearing

Received May 16, 2023
Accepted February 15, 2024